MEASUREMENT NOTES

Note 18

COAXIAL DIELECTRIC WAVEGUIDES II

August 1973

R. DeVore

The Ohio State University ElectroScience Laboratory
Department of Electrical Engineering
Columbus, Ohio 43212

Abstract

Coaxial dielectric waveguides were investigated in order to ascertain their useful bandwidth. The operating bandwidth is defined as a region of dominant HE_{11} mode propagation only, and where 93% or more of the electromagnetic energy is transported internally. Guide loss characteristics are highly dependent on the loss tangents of the several dielectrics. Coaxial dielectric waveguides have more linear phase characteristics than their hollow metallic counterparts. Cutoff wavenumbers for the four lowest of the higher order modes have been found for a number of combinations of dielectrics.

TABLE OF CONTENTS

I. INTRODUCTION

This note completes the analysis of coaxial dielectric waveguides reported previously in Measurement Note 14 (MN14). In MN14 the general format was established, i.e., cutoff wavenumber determination, dispersion relations and certain design criteria. Only a limited number of guide configurations were considered in some detail. As it is desirable to operate the coaxial dielectric waveguide only in the dominant HE_{11} mode and to constrain most of the energy within the guide to avoid external support complications, these problems are treated herein for a representative range of geometric and dielectric configurations.

Two important observations were made during this study. First, a coaxial dielectric waveguide can be designed to have power loss per unit length comparable to that of metallic rectangular waveguides. (Low loss dielectrics, tan $\delta \approx .0002$ are assumed in this conclusion.) Secondly, the guide supports should be placed in the $\phi = 0$ plane of Fig. 1 as the external power carried in this region was found to be a minimum.

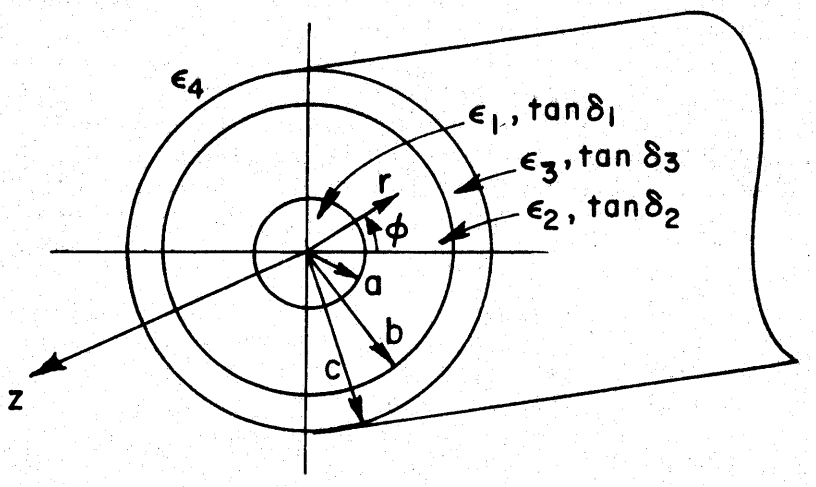

Fig. 1. Coaxial dielectric guide. The field configuration of the dominant HE_{11} mode is similar to the H_{11} conducting hollow cylinder mode. By Eq. (II-46) of MN14, the electric field is oriented "parallel" to the $\phi = 0$ plane.

II. WAVEGUIDE SPECIFICATIONS

The performance of a dielectric waveguide is almost solely a function of the intrinsic dielectric loss or loss tangent. Only realizable configurations have been treated.

Inner rod: $\varepsilon_1 = 2.55$, $\tan \delta_1 = .0002$

Inner tube: $\varepsilon_2 = 1.03$, $\tan \delta_2 = .0002$

Outer tube: $\varepsilon_3 = 2.55$, $\tan \delta_3 = .0002$
$\varepsilon_3 = 2.00$, $\tan \delta_3 = .0002$
$\varepsilon_3 = 4.00$, $\tan \delta_3 = .04$

These appear to be reasonable values according to Reference [1] and the references cited therein. The inner rod, as considered in this note, is always Styron C-176. The inner tube is a low loss polyfoam. Several different outer protective tubes were considered, a low loss polystyrene $\varepsilon_3 = 2.55$, teflon $\varepsilon_3 = 2.00$ and neoprene rubber $\varepsilon_3 = 4.00$. The principal purpose of the outer tube is the prevention of water absorption into the polyfoam which renders the foam tube highly lossy. The waveguide geometry is characterized by Fig. 1. The configurations analyzed are tabulated in Table I.

III. WAVEGUIDE CUTOFF WAVENUMBERS

The first task is to evaluate the modal cutoff expressions given in MN14:

Eq. (34) , E_{01} mode
Eq. (33) , H_{01} mode
Eq. (35) , HE_{12} mode
Eq. (36)$]_{n=2}$, HE_{21} mode

These modes were found to be the lowest of the higher order modes. The guide configurations are specified in terms of their dielectric properties, from inner to outer interface.

2.55 - 1.03 - 2.00
2.55 - 1.03 - 2.55
2.55 - 1.03 - 4.00

The geometric radii ratios are then varied accordingly. For any mode, the boundaries are defined in Fig. 2. The solutions of Eq. (34) for the E_{01} mode are displayed in Figs. 3-5, the solutions of Eq. (33) for the H_{01} mode are shown in Figs. 6-8, the solutions of Eq. (35) for the HE_{12} mode are shown in Figs. 9-11, and the solutions of Eq. (36) for the HE_{21} mode are given in Figs. 12-14. The figures show in greater detail the preliminary results of MN14. The point B of Fig. 2 is not shown as this limit has no practical significance in waveguide design.

TABLE I

COAXIAL DIELECTRIC WAVEGUIDE SUMMARY

Config. No.	Guide Parameters						Cutoffs			
	ε_1	ε_2	ε_3	$\tan\delta_3$	a/c	b/c	E_{01}	H_{01}	HE_{12}	HE_{21}
22	2.55	1.03	2.55	.0002	0.10	0.99	11.15	9.19	9.89	> 12
21					0.15	0.99	10.15	9.07	8.09	> 12
20					0.20	0.975	7.82	6.53	6.39	7.47
23					0.20	0.99	8.45	8.47	7.26	9.61
1					0.25	0.95	6.07	4.88	5.28	5.66
2					0.25	0.975	6.72	6.28	5.89	7.45
15					0.25	0.99	7.01	7.23	6.85	8.47
3					0.30	0.95	5.41	4.75	4.93	5.58
4					0.30	0.975	5.78	5.73	5.60	6.76
16					0.30	0.99	5.95	6.14	6.60	7.25
5					0.35	0.95	4.80	4.51	4.72	5.39
6					0.35	0.975	5.04	5.10	5.43	6.03
17					0.35	0.99	5.16	5.31	6.39	6.29
7	2.55	1.03	2.00	.0002	0.25	0.95	6.33	5.82	5.63	6.59
8					0.25	0.975	6.82	6.93	6.30	7.94
26					0.25	0.99	7.04	7.35	7.21	8.62
9					0.30	0.95	5.56	5.47	5.32	6.35
10					0.30	0.975	5.84	6.02	6.04	7.07
11					0.35	0.95	4.90	4.96	5.12	5.88
12					0.35	0.975	5.08	5.24	5.86	6.39
18	2.55	1.03	4.00	.04	0.25	0.95	5.70	3.62	4.87	4.35
19				.04	0.25	0.975	6.57	4.89	5.30	5.82
25				.04	0.25	0.99	6.97	6.68	6.21	7.89
13				.04	0.30	0.95	5.18	3.59	4.43	4.34
13A				.0002	0.30	0.95				
14				.04	0.30	0.975	5.70	4.76	4.97	5.91
24				.04	0.30	0.99	5.92	5.92	5.95	7.06

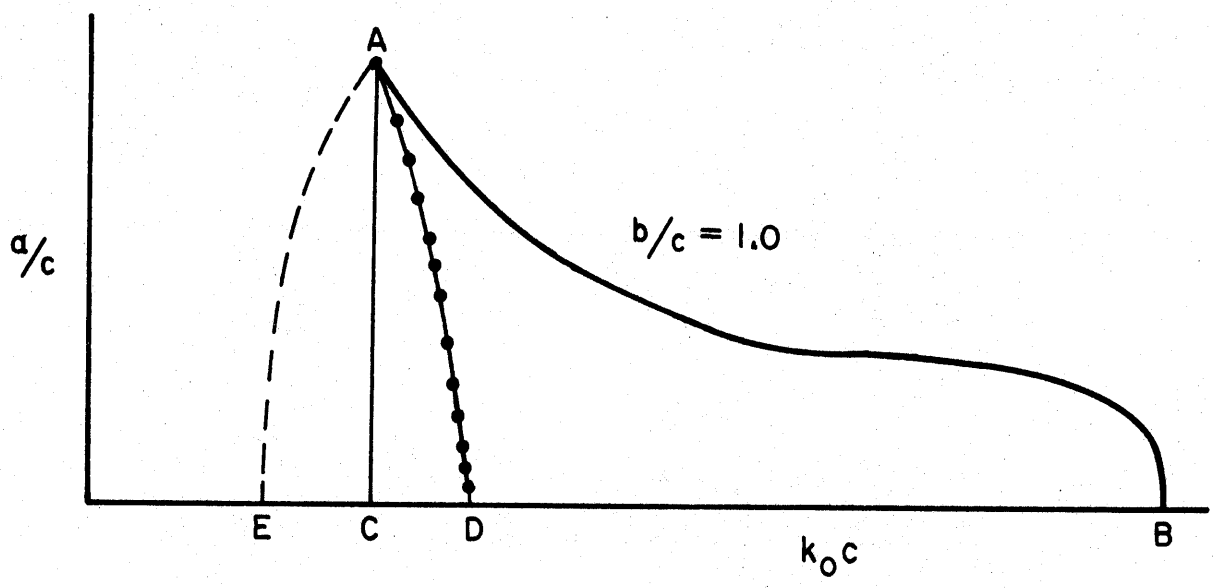

Fig. 2. Geometric boundaries for cutoff wavenumbers of the coaxial dielectric modes.

Point A: Cutoff for ε_1 = 2.55 rod
Path AB: Cutoff ε_1 = 2.55 rod clad by ε_2 = 1.03 foam tube (b/c = 1.0)
Point B: Cutoff for ε_2 = 1.03 rod
Path BC: Cutoff ε_2 = 1.03 rod clad by ε_3 = 2.55 tube
Path BD: Cutoff ε_2 = 1.03 rod clad by ε_3 = 2.00 tube
Path BE: Cutoff ε_2 = 1.03 rod clad by ε_3 = 4.00 tube
Point C: ε_3 = 2.55 rod cutoff
Point D: ε_3 = 2.00 rod cutoff
Point E: ε_3 = 4.00 rod cutoff
Path CA: $\varepsilon_1 = \varepsilon_3$ = 2.55 rod cutoff (a = b)
Path DA: ε_1 = 2.55 rod clad by ε_3 = 2.00 tube (a = b)
Path EA: ε_1 = 2.55 rod clad by ε_3 = 4.00 tube (a = b)

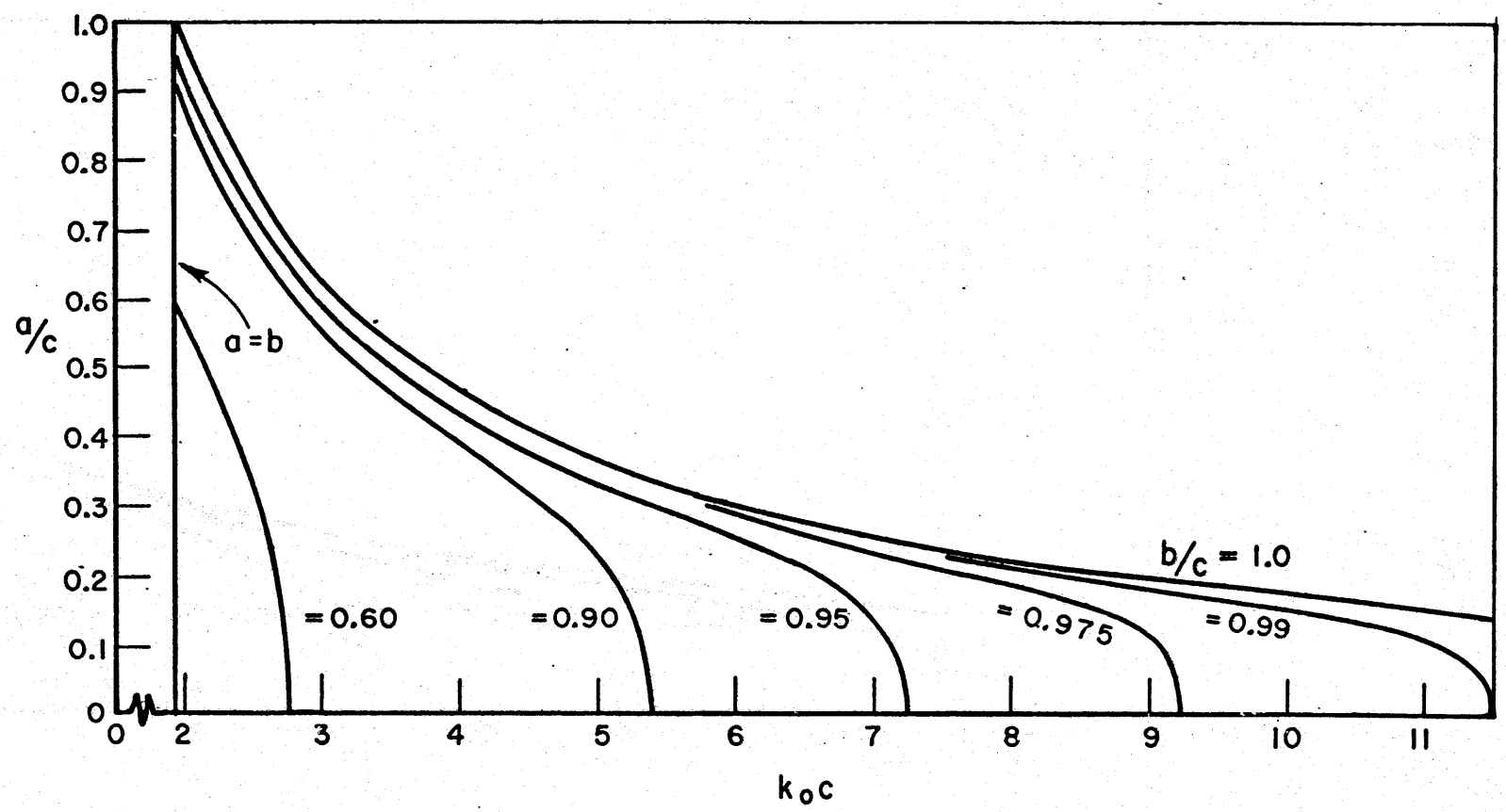

Fig. 3. Radii ratio (a/c) vs cutoff wavenumber $\varepsilon_1=\varepsilon_3=2.55$, $\varepsilon_2=1.03$ [E_{01}, Eq. (34)].

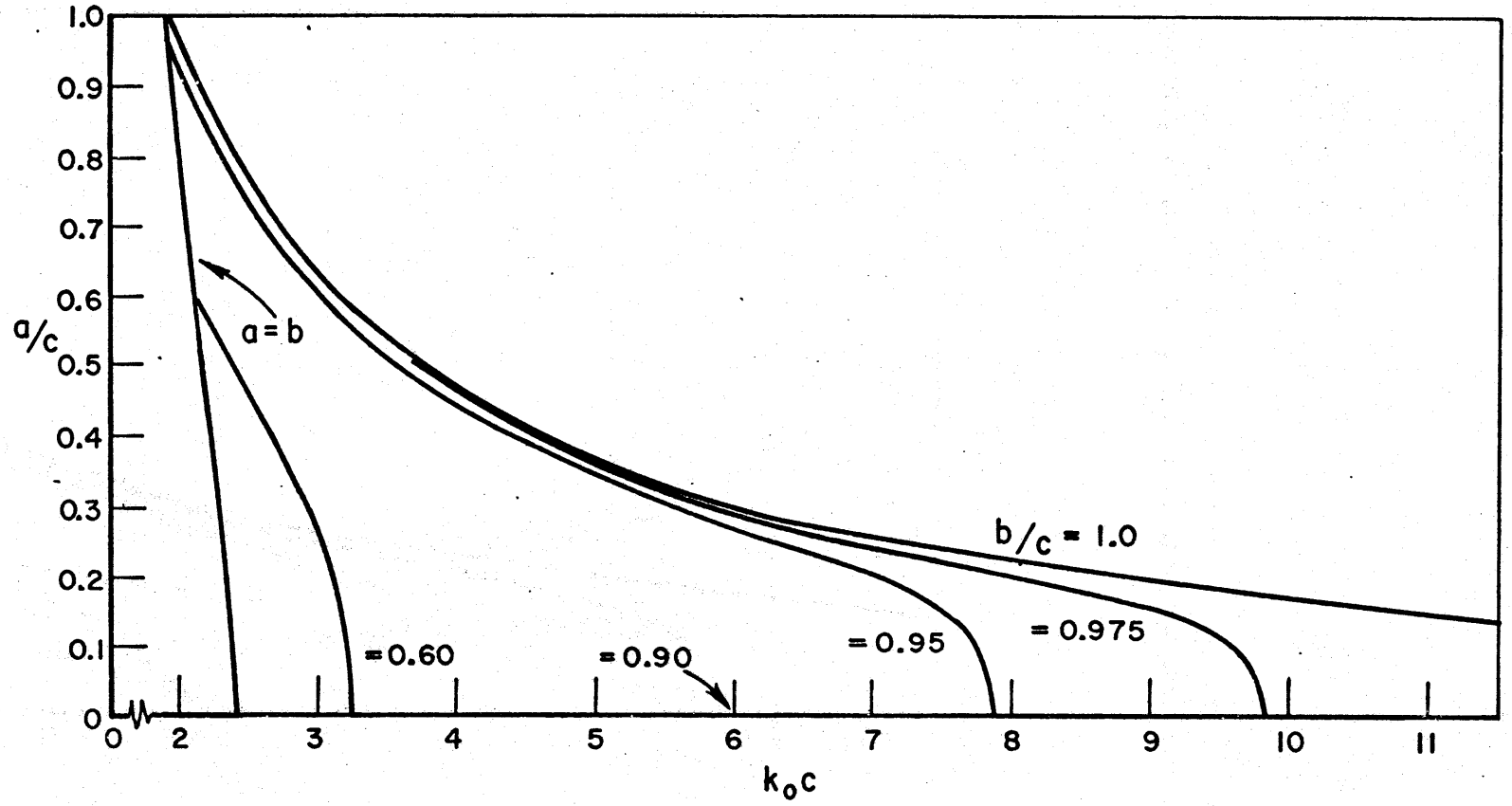

Fig. 4. Radii ratio (a/c) vs cutoff wavenumber $\varepsilon_1=2.55$, $\varepsilon_2=1.03$, $\varepsilon_3=2.00$ [E_{01}, Eq. (34)].

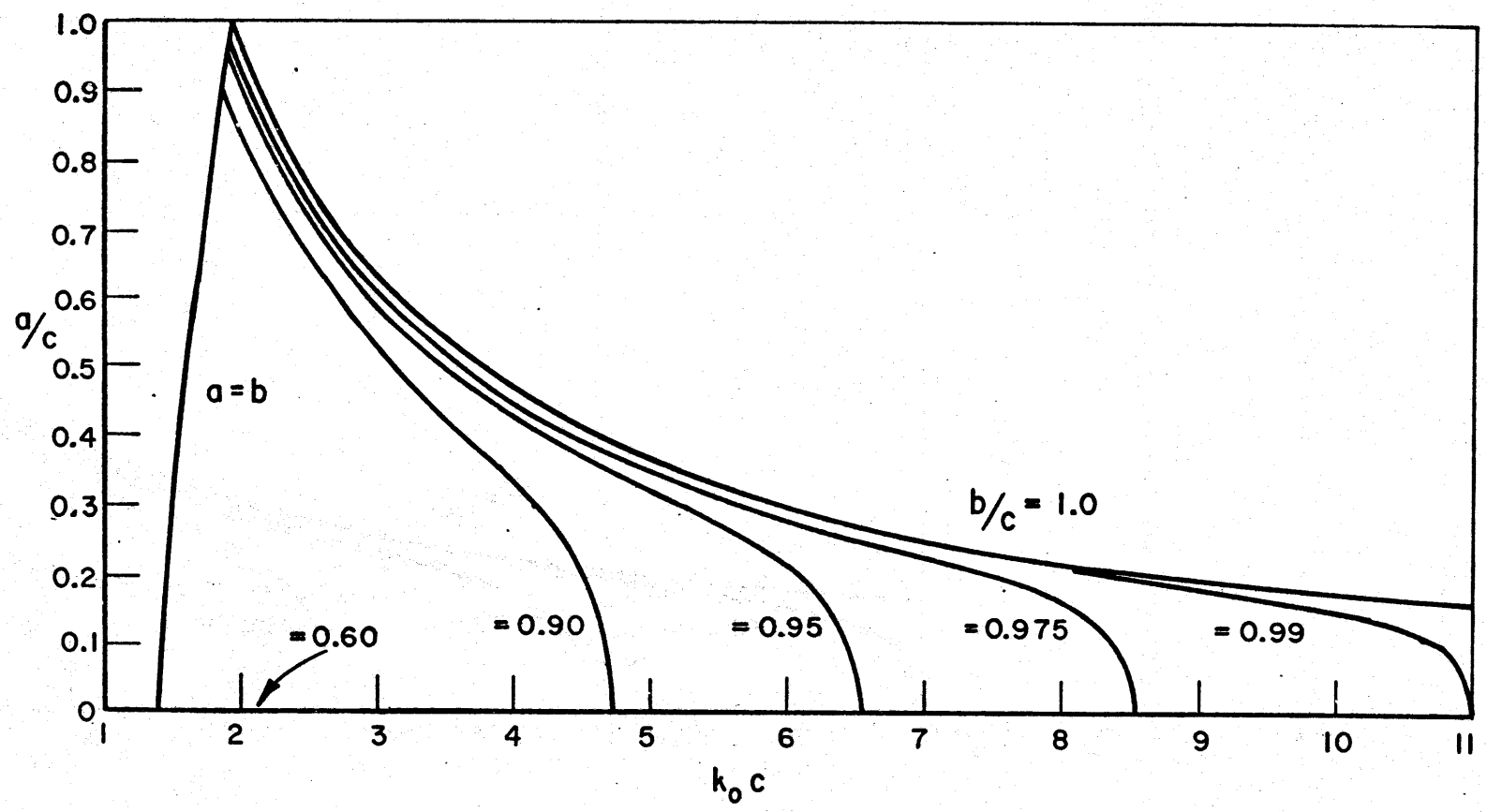

Fig. 5. Radii ratio (a/c) vs cutoff wavenumber ε_1=2.55, ε_2=1.03, ε_3=4.00 [E_{01}, Eq. (34)].

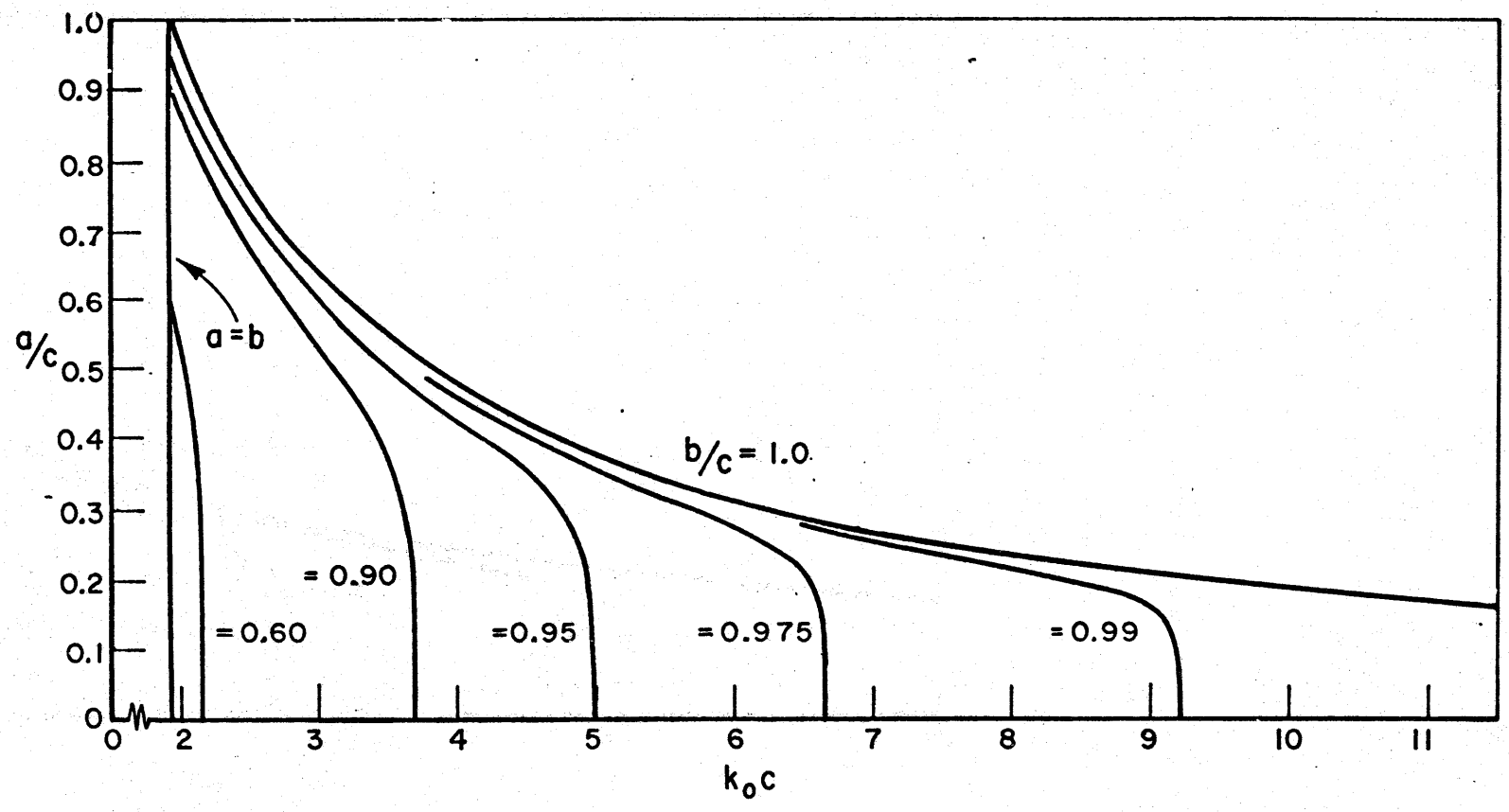

Fig. 6. Radii ratio (a/c) vs cutoff wavenumber $\varepsilon_1=\varepsilon_3=2.55$, $\varepsilon_2=1.03$ [H_{01}, Eq. (33)].

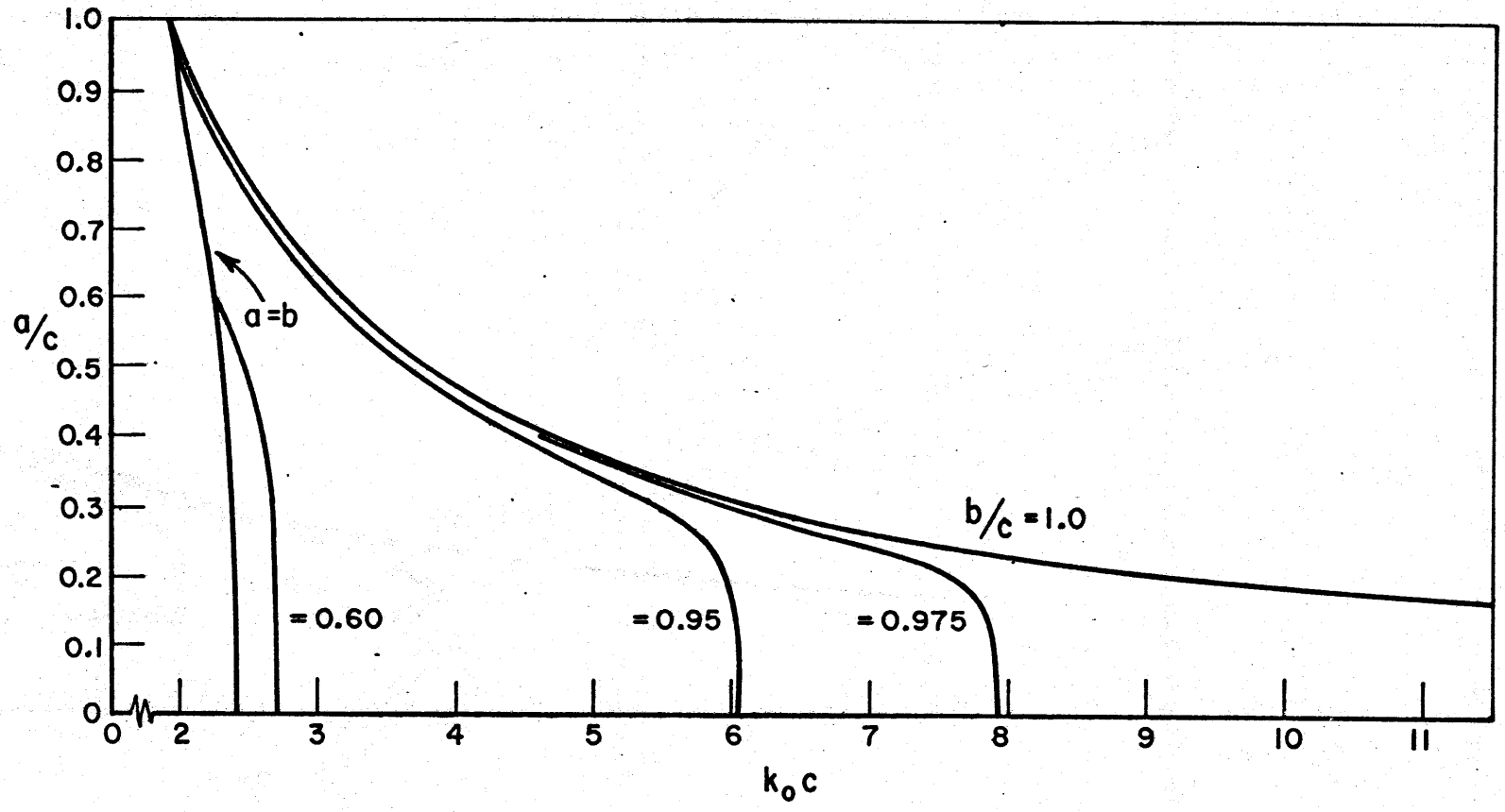

Fig. 7. Radii ratio (a/c) vs cutoff wavenumber ε_1=2.55, ε_2=1.03, ε_3=2.00 [H_{01}, Eq. (33)].

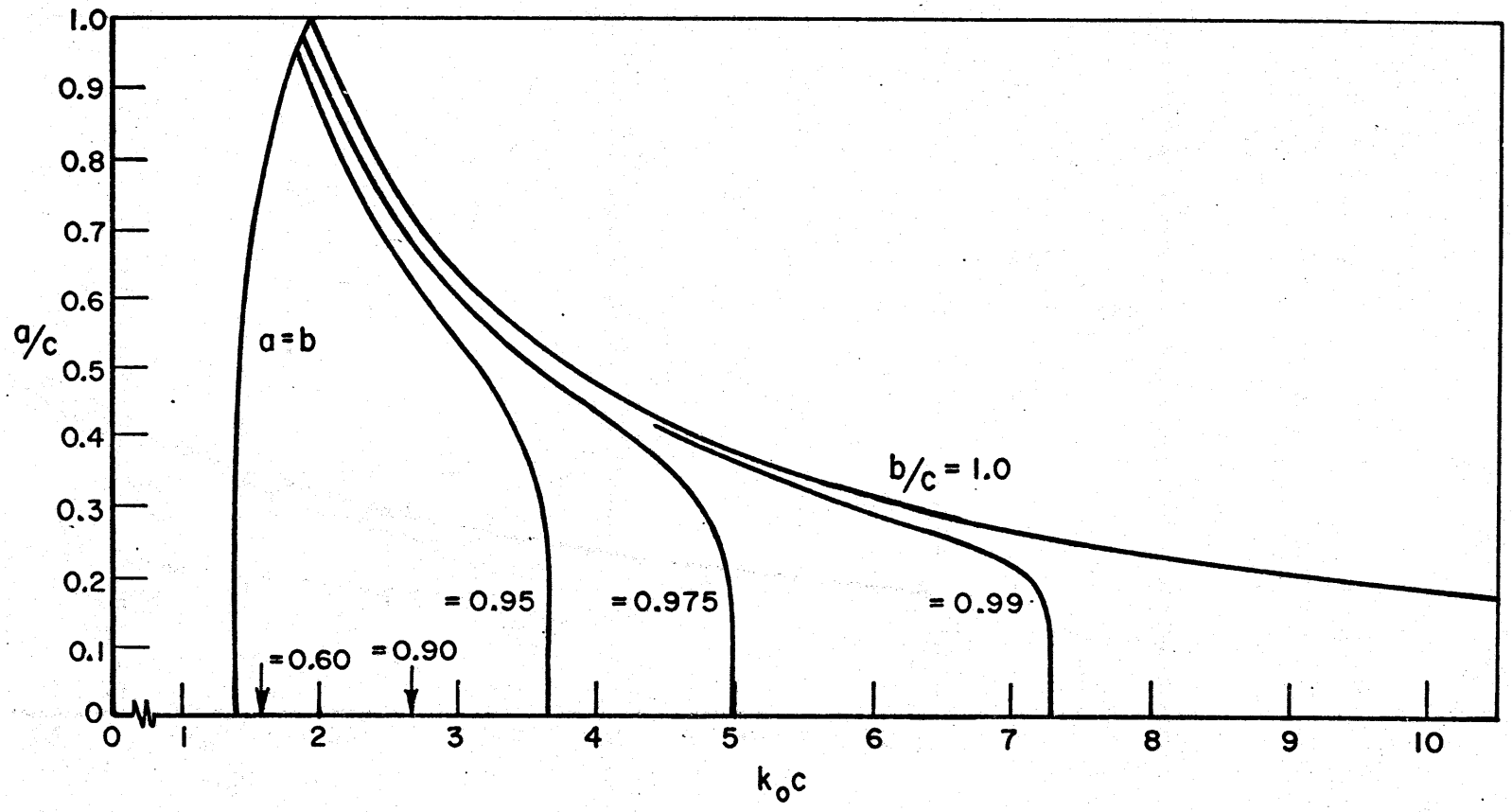

Fig. 8. Radii ratio (a/c) vs cutoff wavenumber ε_1=2.55, ε_2=1.03, ε_3=4.00 [H_{01}, Eq. (33)].

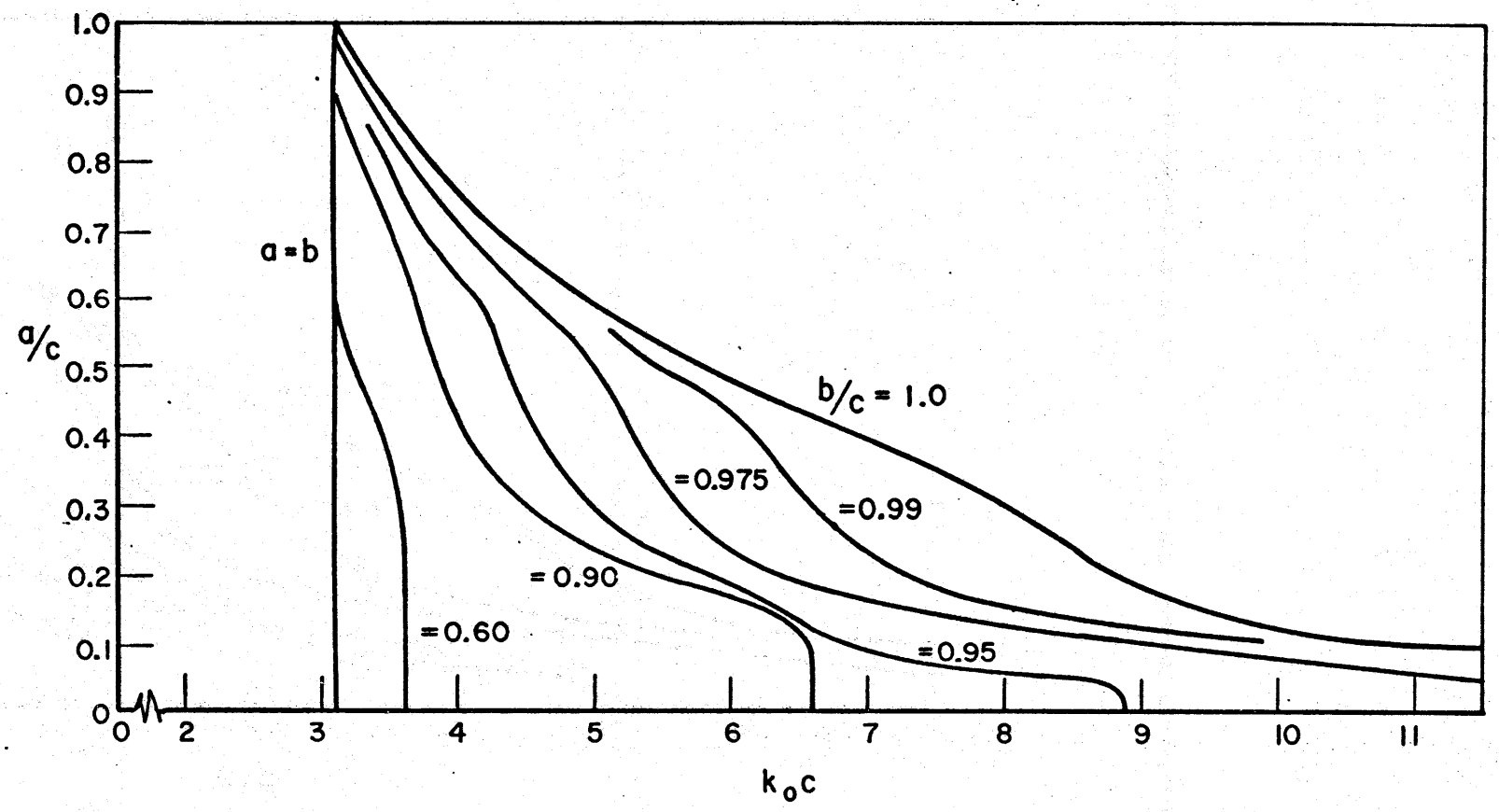

Fig. 9. Radii ratio (a/c) vs cutoff wavenumber $\varepsilon_1=\varepsilon_3=2.55$, $\varepsilon_2=1.03$ (HE_{12}, Eq. (35)].

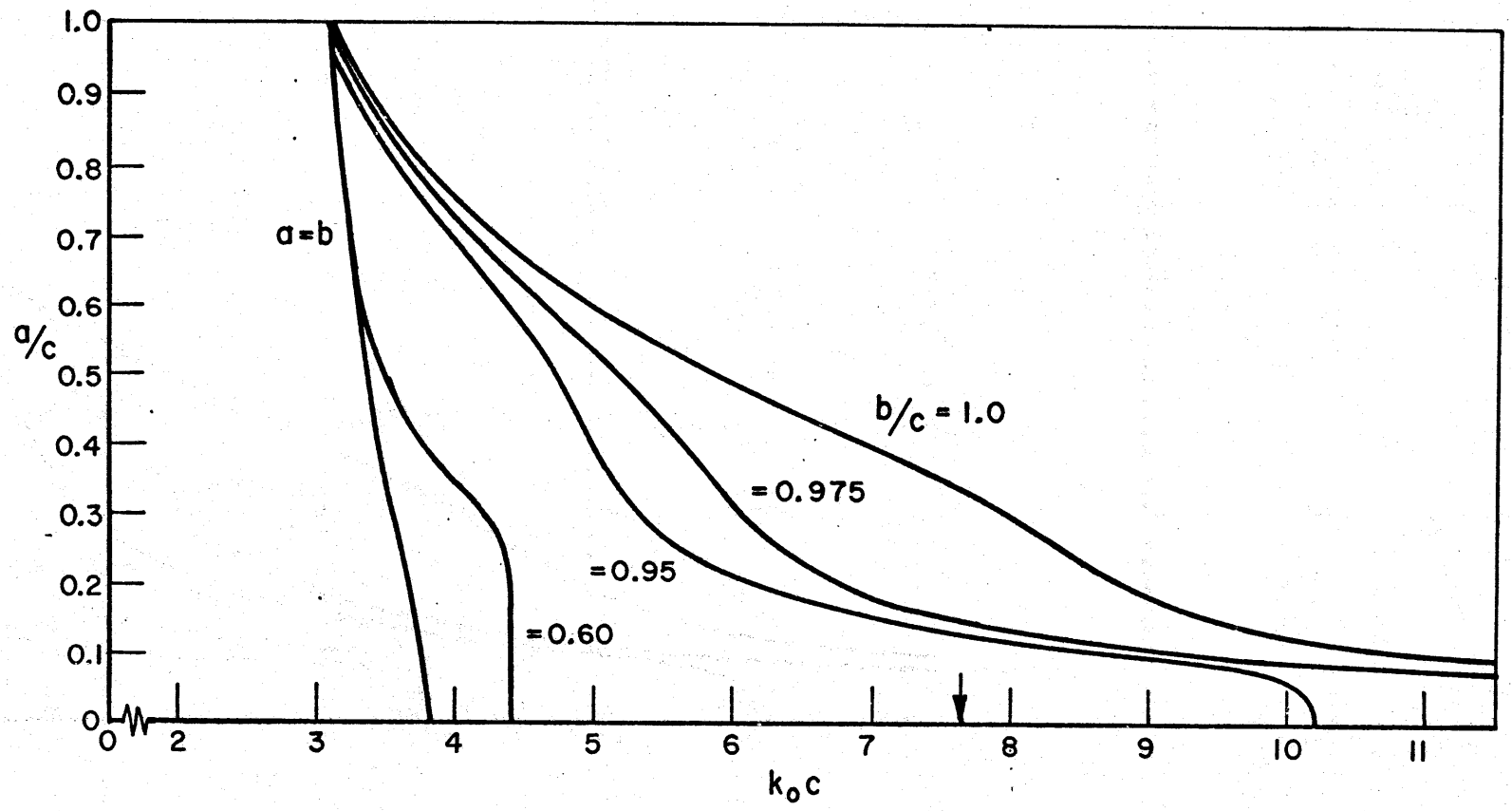

Fig. 10. Radii ratio (a/c) vs cutoff wavenumber ε_1=2.55, ε_2=1.03, ε_3=2.00 [HE_{12}, Eq. (35)].

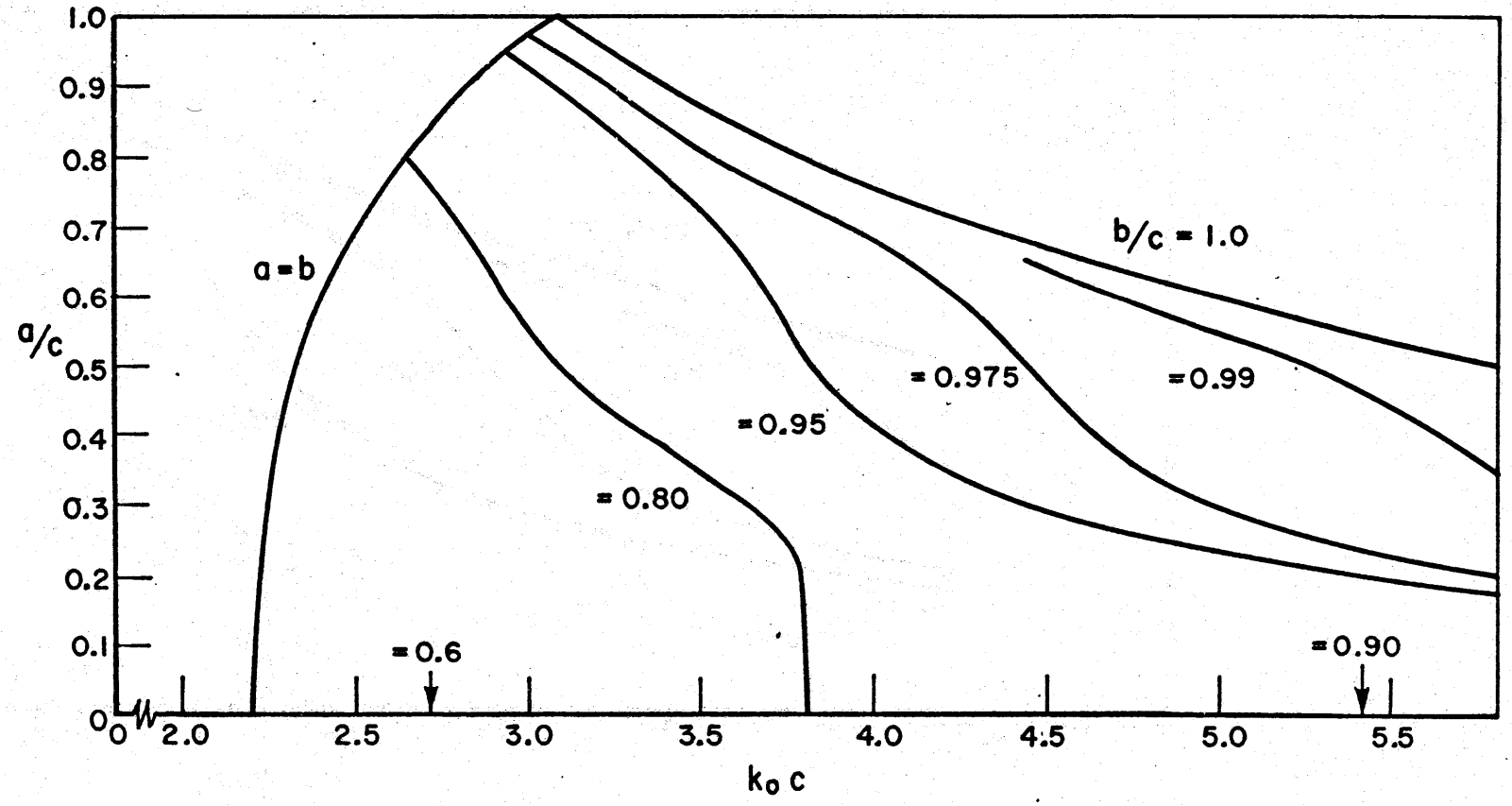

Fig. 11. Radii ratio (a/c) vs cutoff wavenumber ε_1=2.55, ε_2=1.03, ε_3=4.00 [HE_{12}, Eq. (35)].

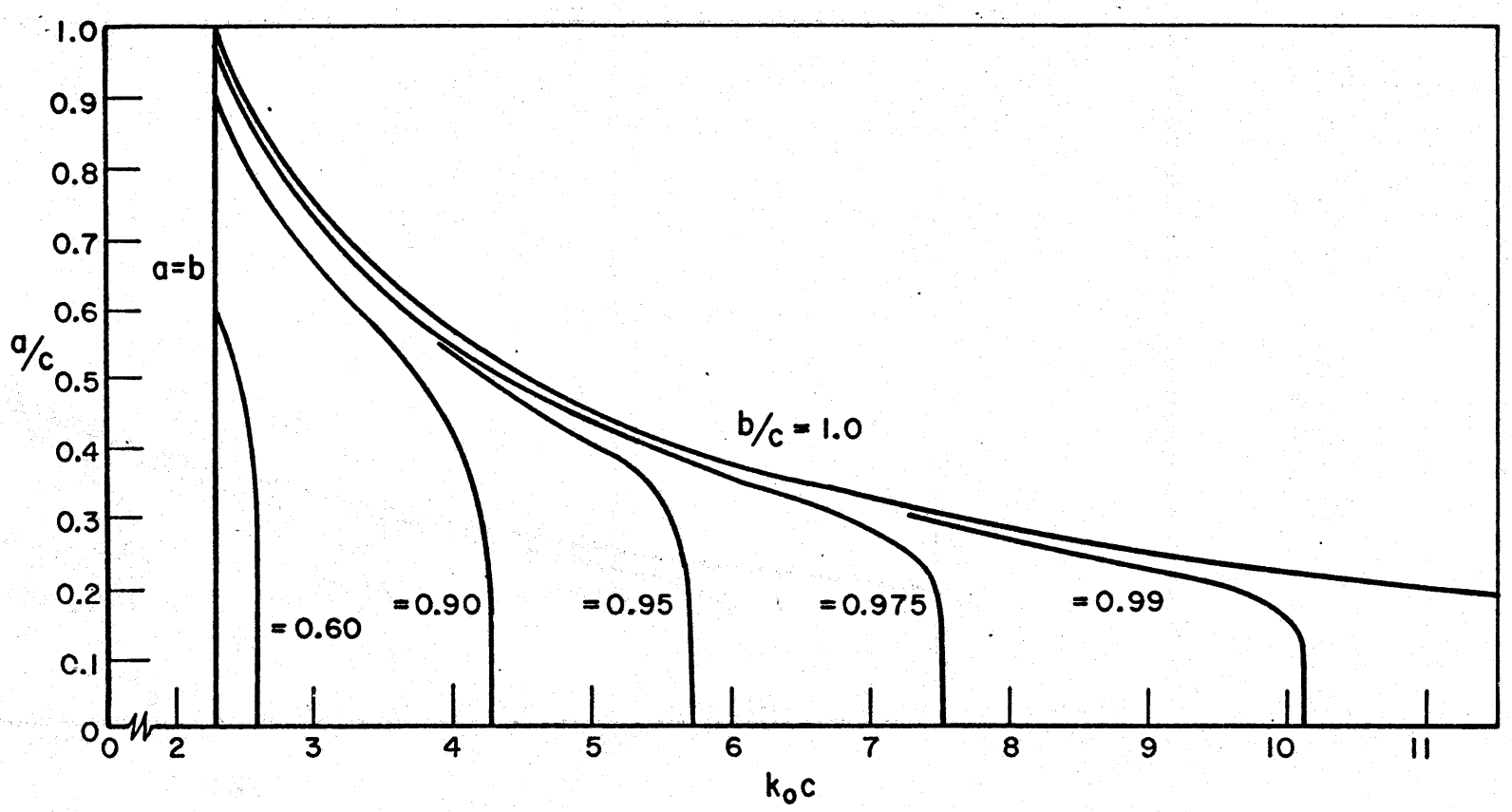

Fig. 12. Radii ratio (a/c) vs cutoff wavenumber $\varepsilon_1=\varepsilon_3=2.55$, $\varepsilon_2=1.03$ [HE_{21}, Eq. (36)].

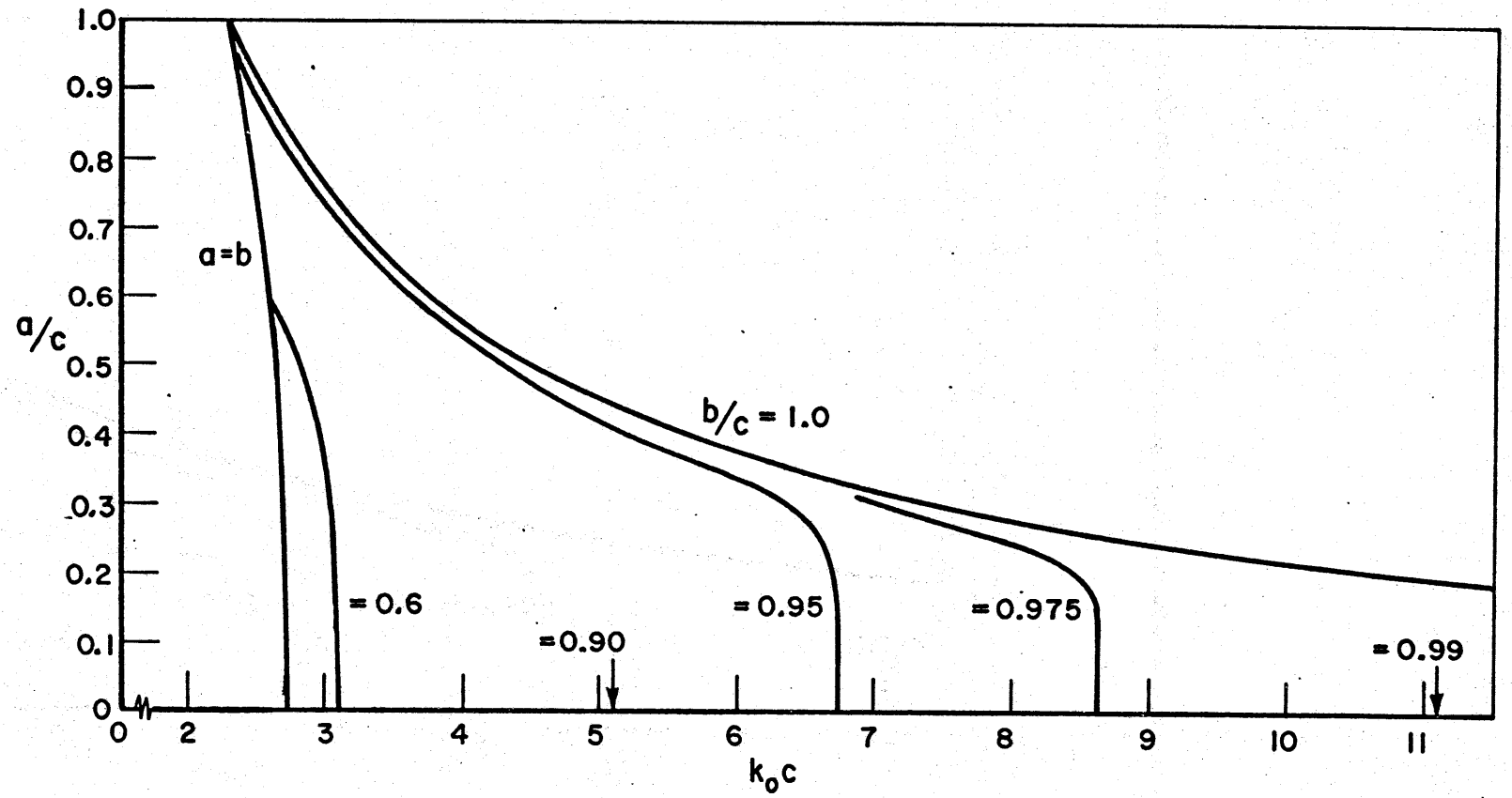

Fig. 13. Radii ratio (a/c) vs cutoff wavenumber ε_1=2.55, ε_2=1.03, ε_3=2.00 [HE_{21}, Eq. (36)].

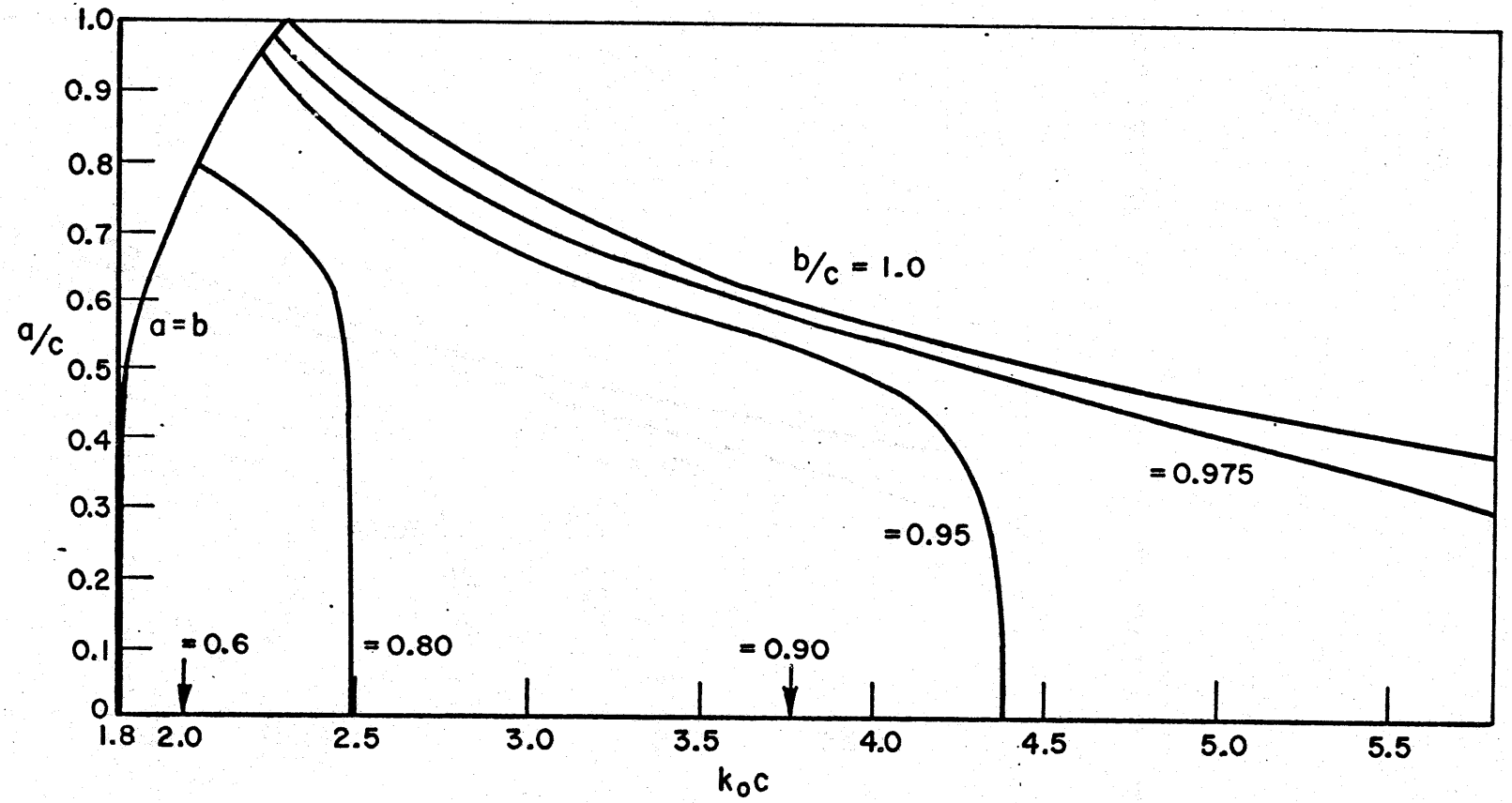

Fig. 14. Radii ratio (a/c) vs cutoff wavenumber ε_1=2.55, ε_2=1.03, ε_3=4.00 [HE_{21}, Eq. (36)].

IV. DISPERSION AND ATTENUATION

Attenuation and dispersion data for the dominant HE_{11} mode for the various configurations of Table I are found upon evaluating Eq. (II-49) of MN14 for the case n = 1. Figs. 15 and 16 show the results for the 2.55-1.03-2.55 dielectrics, Figs. 17 and 18 for the 2.55-1.03-2.00 dielectrics and Figs. 19 and 20 for the 2.55-1.03-4.00 dielectric ordering. The appearance of the first higher order mode is indicated on all of the characteristics.

At this point the importance of dielectric loss is apparent. Comparison of the attenuation characteristics of Fig. 19 with those of Figs. 15 and 17 clearly demonstrate the effect of a lossy neoprene outer protective tube. Fig. 19 is also interesting from the standpoint of an absorption resonance. It was noted that the external power distribution was quite asymmetrical about the absorption maximum. Also, this is the transition region where the guide is beginning to transport more energy internally than externally.

The attenuation characteristics have not been normalized as was done in MN14. The asymptotic values for all dispersion and attenuation characteristics are their infinite medium ($\varepsilon_1 = 2.55$) values; i.e.,

$$\gamma/k_0 \sim \sqrt{\varepsilon_1} = \sqrt{2.55(1-j.0002)} \approx 1.597 - j.00016 \quad .$$

A comparison of attenuation characteristics with those of rectangular metallic guides, shown in Fig. 21 for X, K_u and K_a bands, is worthwhile. The dielectric guide attenuation in db per meter is

$$\text{Attenuation} = 8.686\, k_0\, |\text{Im}\, \gamma/k_0|$$

where k_0 is expressed in units of reciprocal meters. As both k_0 and $|\text{Im}\, \gamma/k_0|$ increase with frequency, then dielectric waveguide attenuation is a monotonically increasing function of frequency while metallic guide attenuation is a decreasing function over any useful bandwidth. A qualitative comparison will follow after a discussion of energy confinement.

V. AXIAL ENERGY TRANSPORT

Referring to Fig. 1, it is seen that electromagnetic energy is necessarily transported in all four regions. For practical reasons it is desirable to carry the preponderance of axial power in regions 1 and 2. This objective is easily achievable, however, higher order modes are then excited. By Eqs. (5) and (6) of MN14, the time average power density in the axial direction is

$$(1) \qquad S_z(r,\phi) = \tfrac{1}{2}\text{Re}\left[E_r H_\phi^* - E_\phi H_r^*\right] = F(r)\cos^2\phi + G(r)\sin^2\phi$$

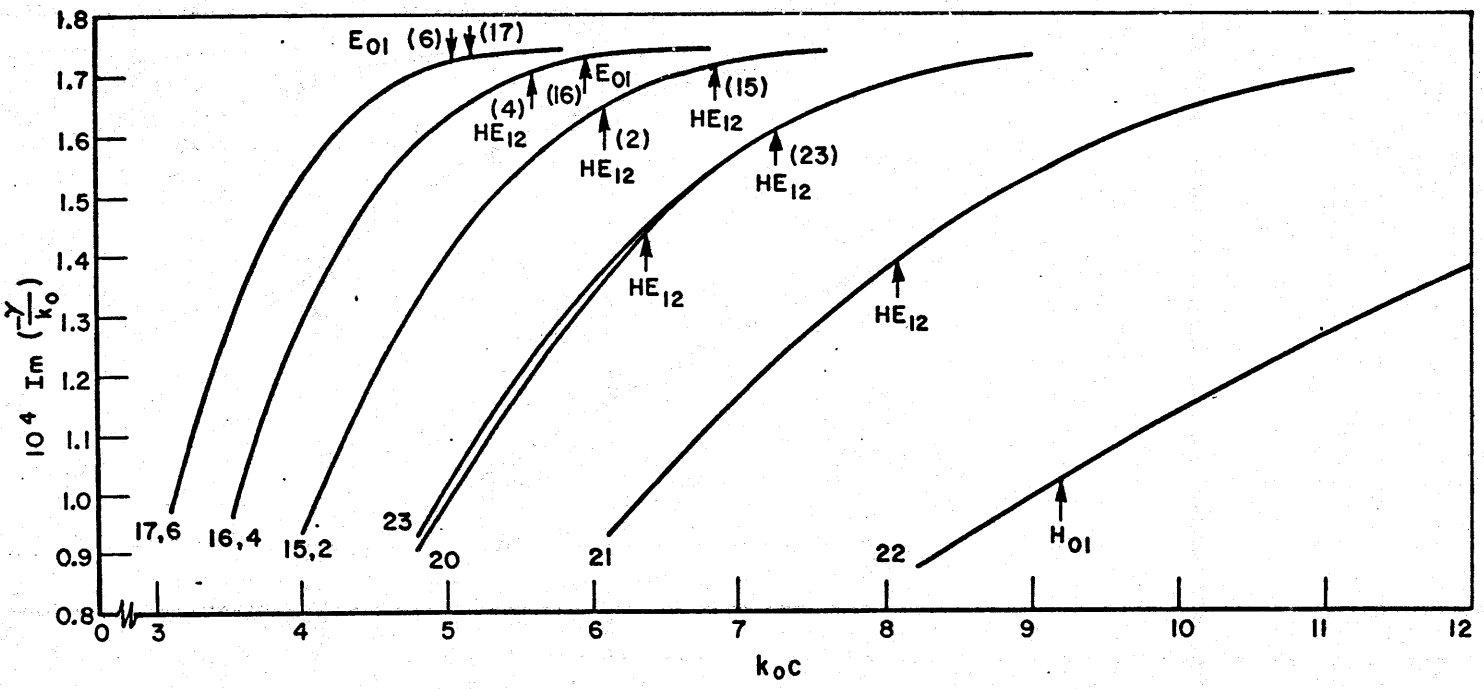

Fig. 15. Attenuation characteristics for HE_{11} mode $\varepsilon_1=\varepsilon_3=2.55$, $\varepsilon_2=1.03$. Numbers labeling curves refer to configurations identified in Table I. Appearance of first higher order mode indicated.

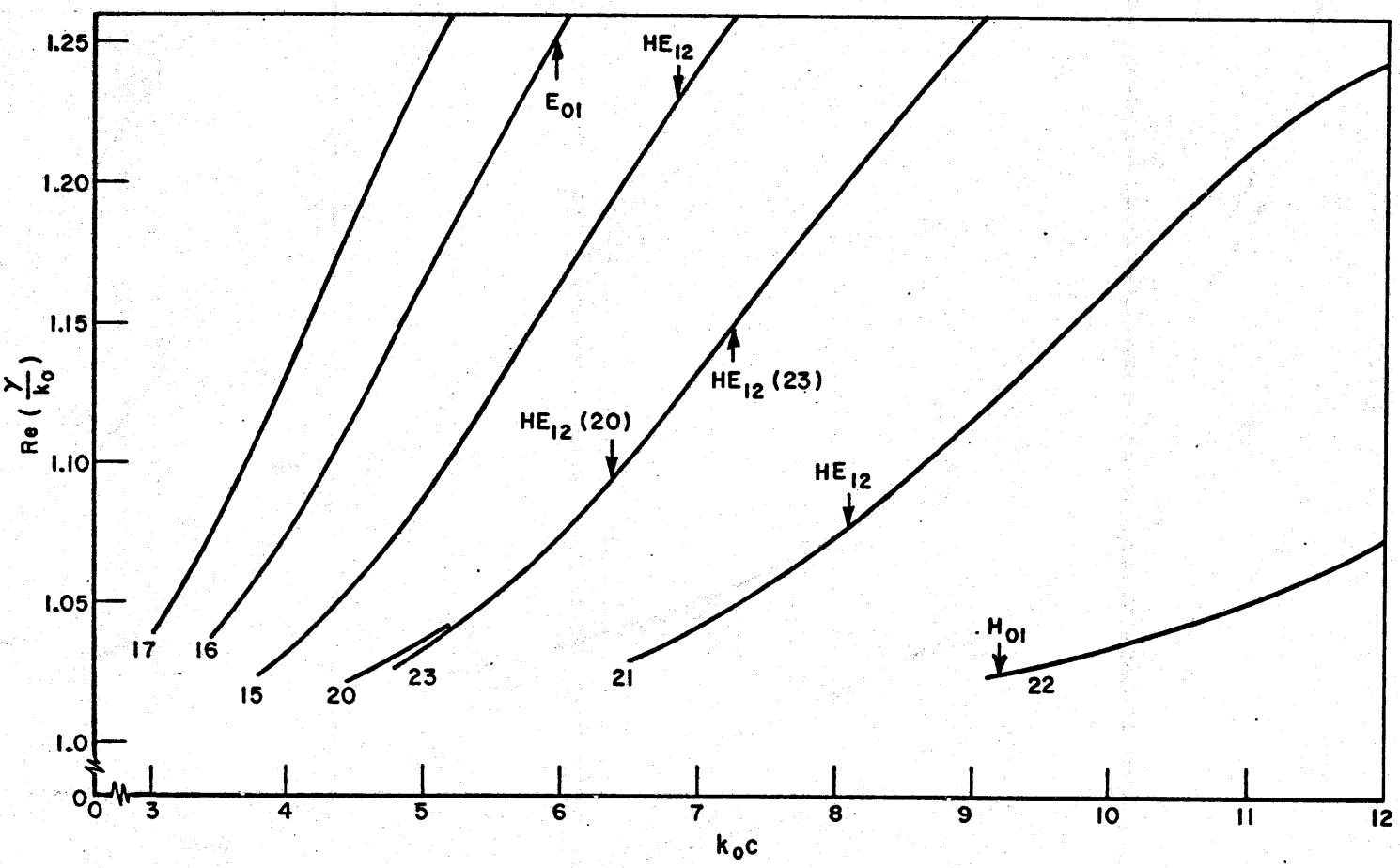

Fig. 16. Dispersion characteristics for HE_{11} mode $\varepsilon_1=\varepsilon_3=2.55$, $\varepsilon_2=1.03$. Numbers labeling curves refer to configurations identified in Table I. Appearance of first higher order mode indicated.

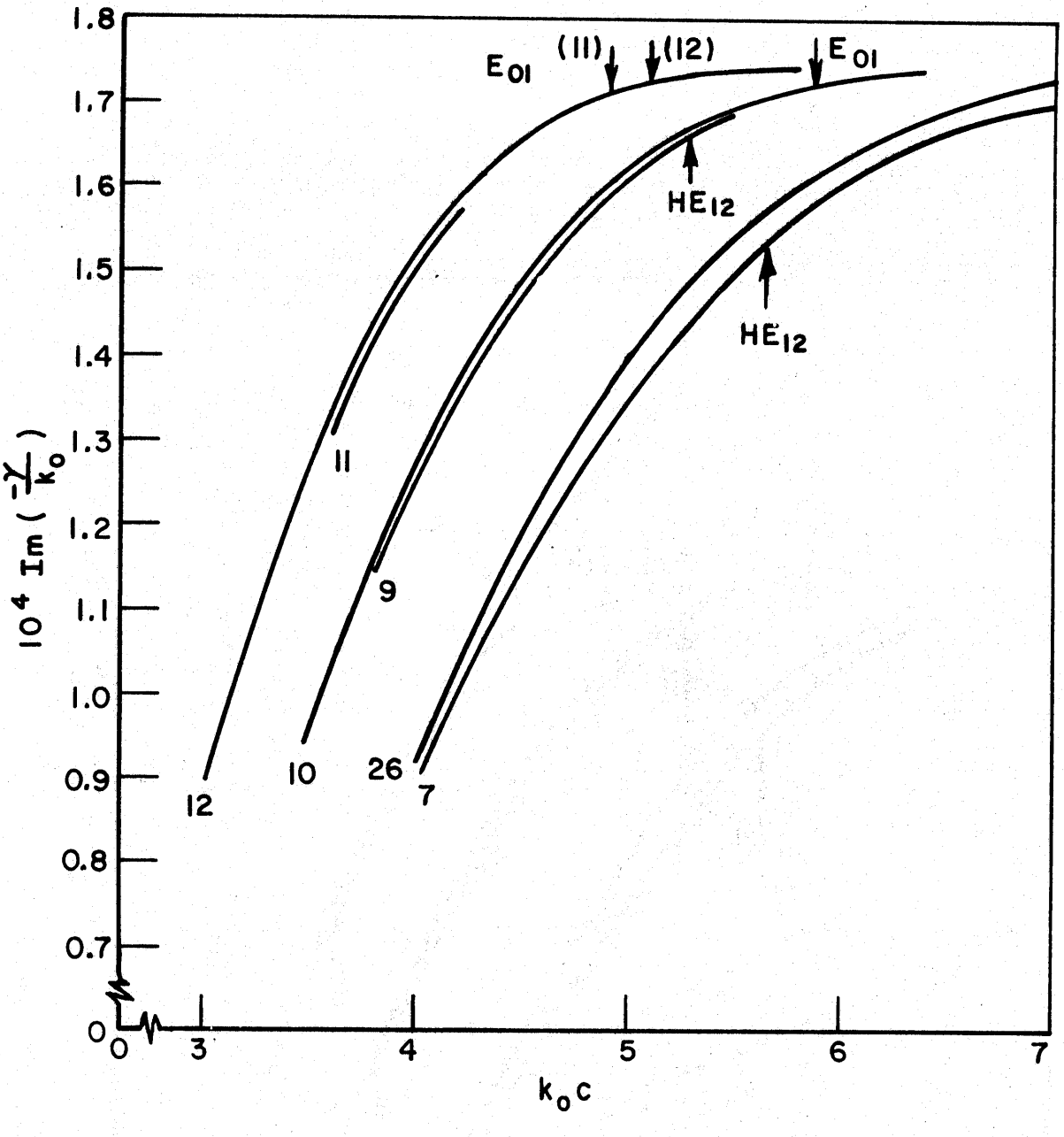

Fig. 17. Attenuation characteristics for HE_{11} mode $\varepsilon_1=2.55$, $\varepsilon_2=1.03$, $\varepsilon_3=2.00$. Numbers labeling curves refer to configurations identified in Table I. Appearance of first higher order mode indicated.

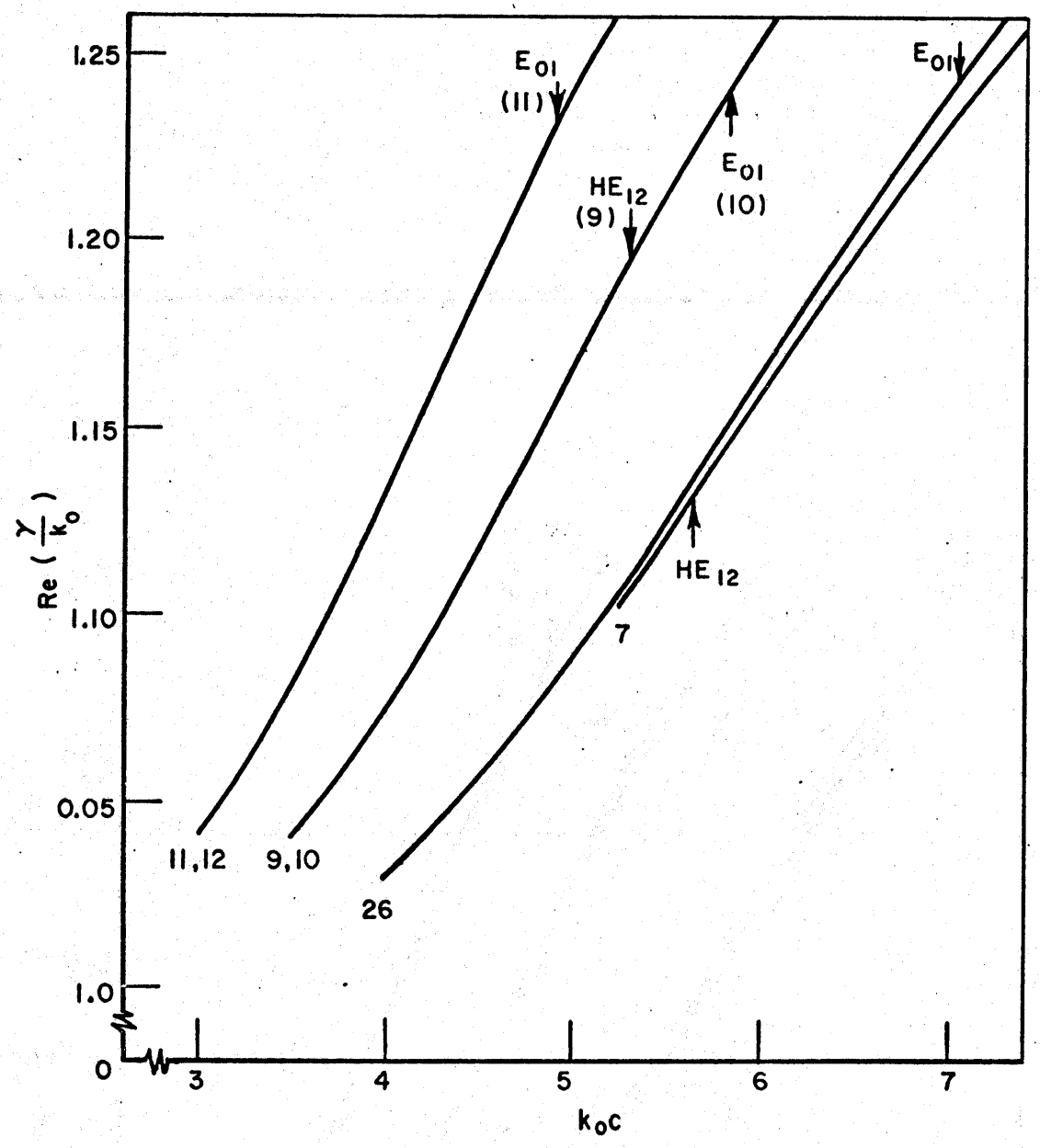

Fig. 18. Dispersion characteristics for HE_{11} mode $\varepsilon_1=2.55$, $\varepsilon_2=1.03$, $\varepsilon_3=2.00$. Numbers labeling curves refer to configurations identified in Table I. Appearance of first higher order mode indicated.

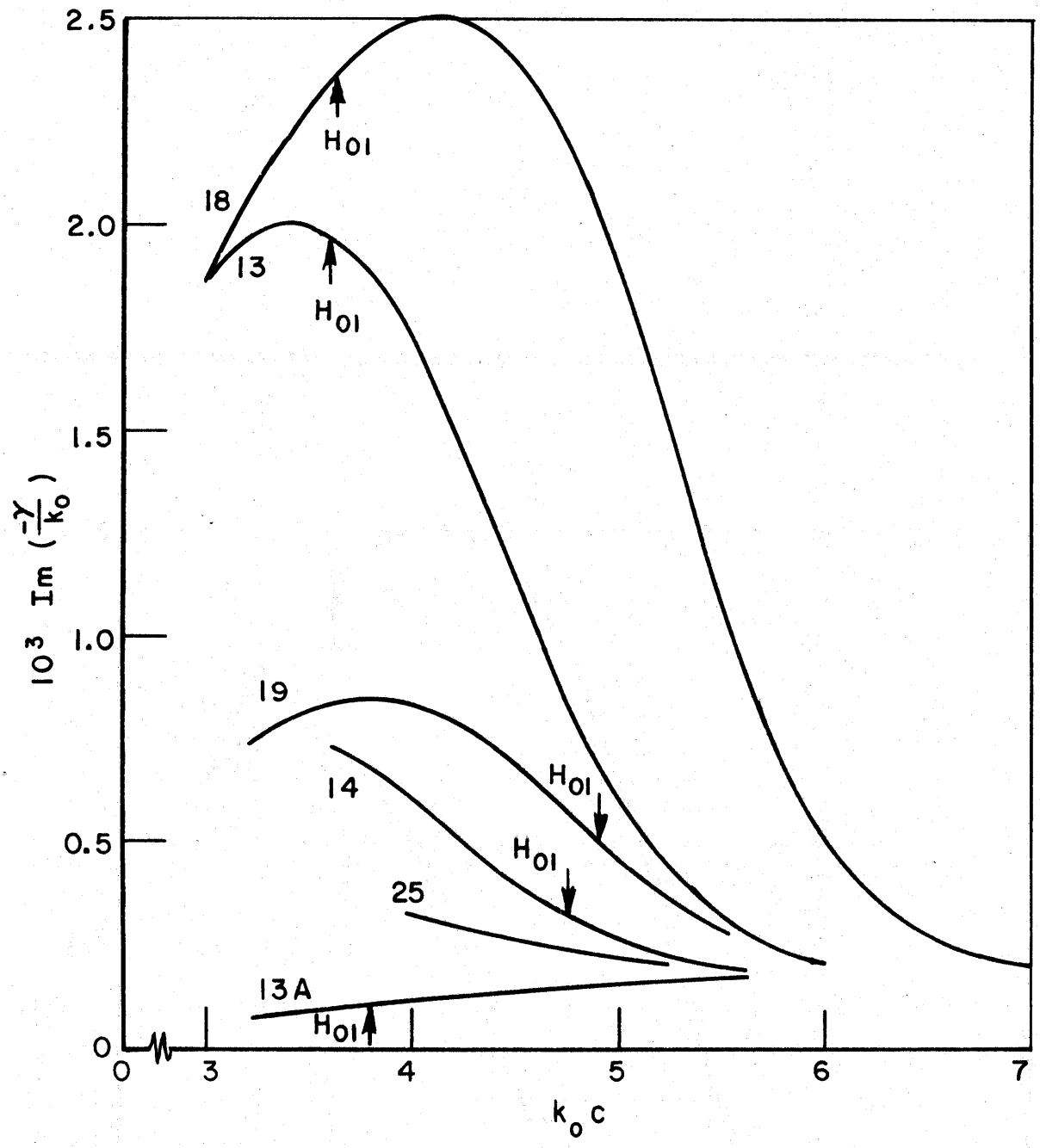

Fig. 19. Attenuation characteristics for HE_{11} mode ε_1=2.55, ε_2=1.03, ε_3=4.00. Numbers labeling curves refer to configurations identified in Table I. Appearance of first higher order mode indicated.

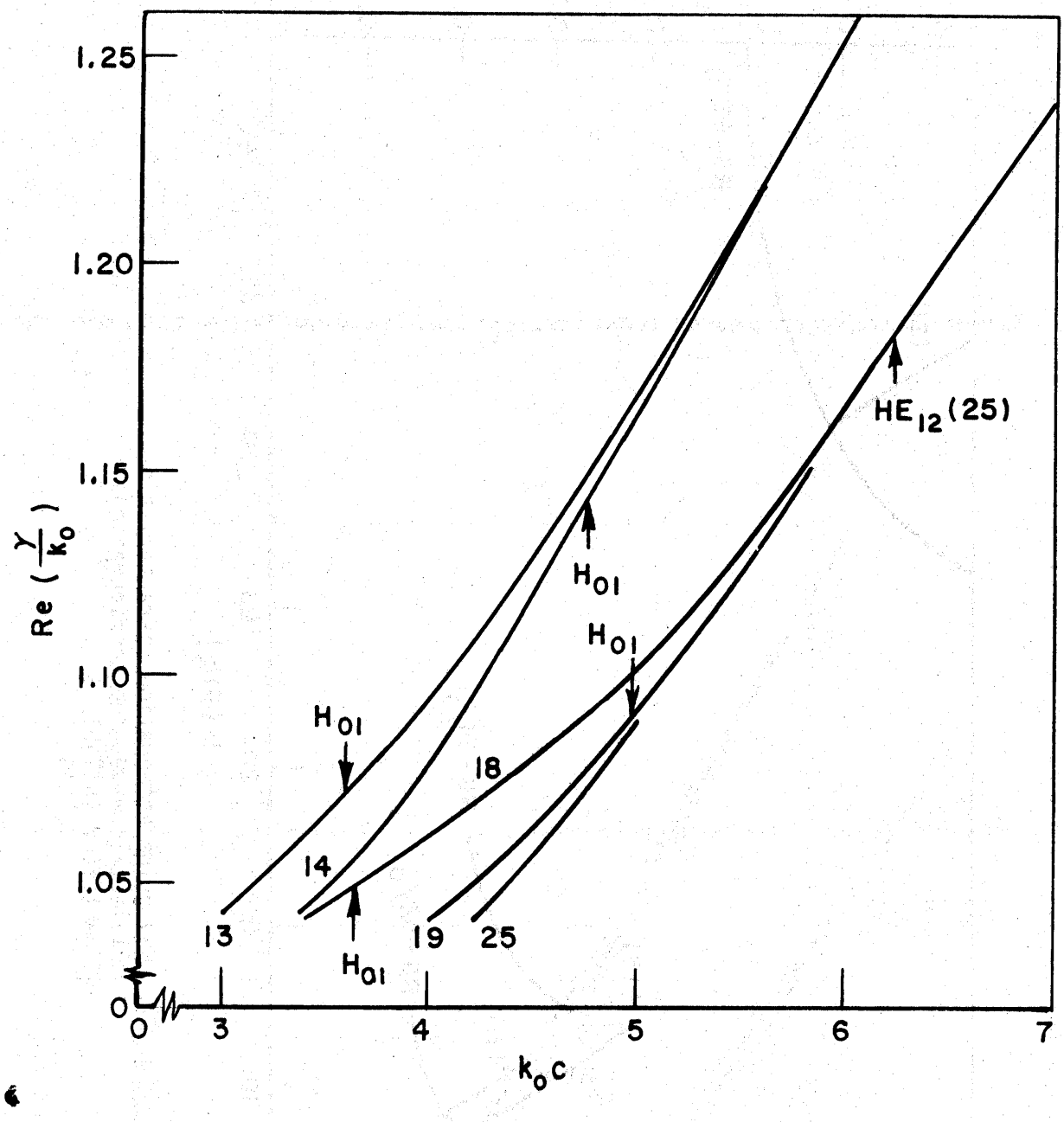

Fig. 20. Dispersion characteristics for HE_{11} mode $\varepsilon_1=2.55$, $\varepsilon_2=1.03$, $\varepsilon_3=4.00$. Numbers labeling curves refer to configurations identified in Table I. Appearance of first higher order mode indicated.

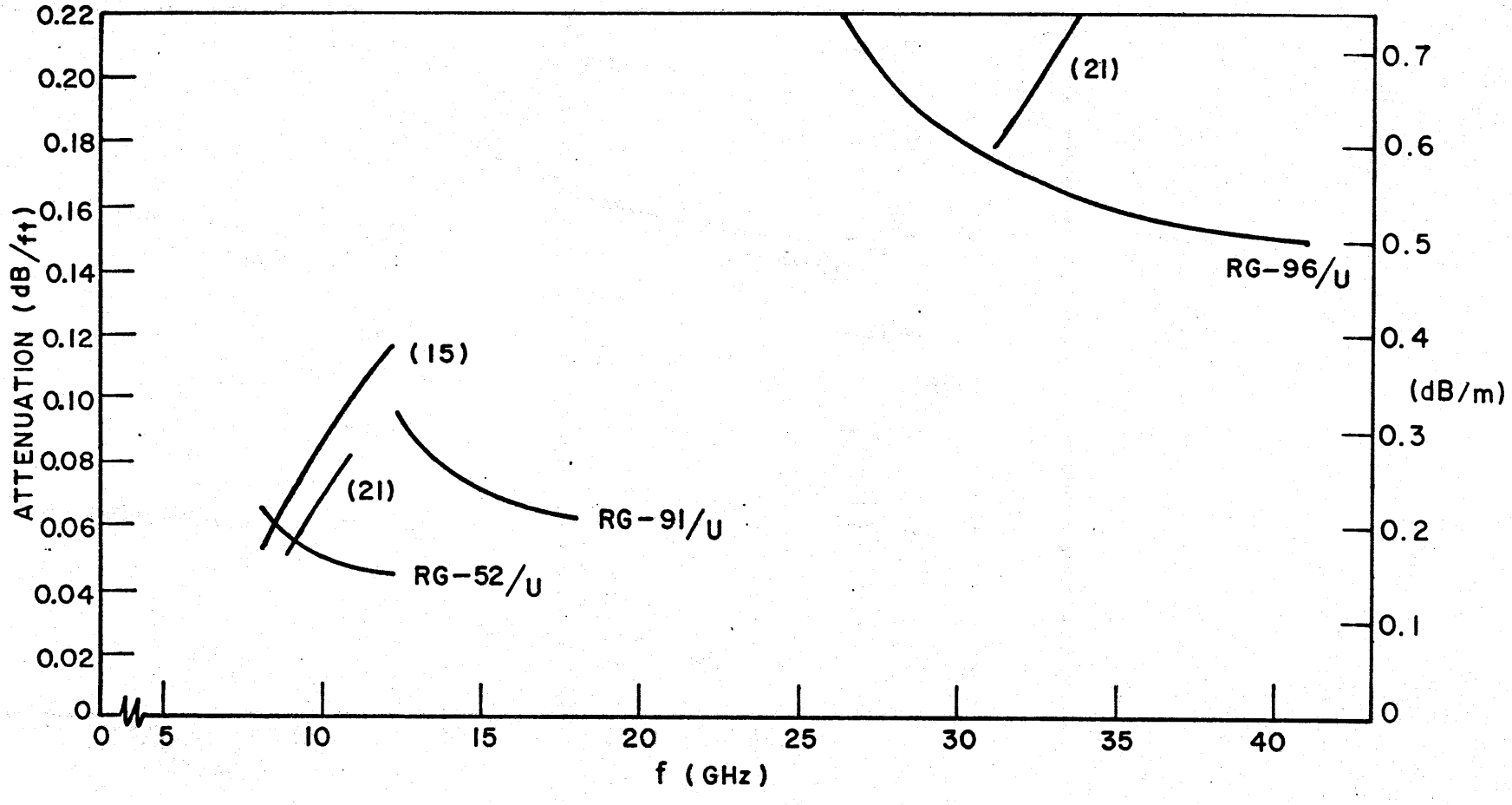

Fig. 21. Waveguide attenuation characteristics. Dielectric waveguide configurations identified in Table I.

The function $F(r)$ is the power distribution in the $\phi = 0$ plane and $G(r)$ is similarly defined for the $\phi = \pi/2$ plane (see Fig. 1). Using Eqs. (II-45) to (II-48) of MN 14, $S_z(r,\phi)$ is evaluated over a transverse cross section. We define the ratio of internal to total axial power transported to be

$$(2) \qquad \frac{P_{int}}{P_{tot}} = \left[\int_o^c \{F(r) + G(r)\}\, r\, dr\right] \left[\int_o^\infty \{F(r) + G(r)\} r\, dr\right]^{-1}$$

The results of these calculations are shown in Figs. 22-24. Again, the appearance of the first higher mode is labeled on the various curves. Most of the important data is now available so we can examine the performance of several waveguides.

Before doing this, one observation made during the calculations is worth a comment. It was found that in the regions of practical guide operation the following was generally true (b is the inner radius of the outer tube).

$$(3) \qquad \left[\int_o^\infty F(r)\, r\, dr\right] \left[\int_b^\infty G(r)\, r\, dr\right]^{-1} < 1$$

The frequency dependence is shown in Fig. 25 for configuration 15 of Table I. It does seem worthwhile to support the guide in the $\phi = 0$ plane of Fig. 1. Earlier it was mentioned that under particular conditions the power distribution was asymmetrical. This is not the case for any useful guide as seen upon inspection of Fig. 25 where Eq. (3) is evaluated for $b = 0$.

VI. WAVEGUIDE PERFORMANCE

Establishing dual requirements that the guide must propagate the dominant HE_{11} mode only, and that 93% or more of the power must be internally transported, we summarize the operating regions of some of the more promising configurations in Table II. A close inspection of the figures leads to several observations.

1. A thin outer protective tube ($b/c = 0.99$) provides greater bandwidth than the thicker outer tubes.

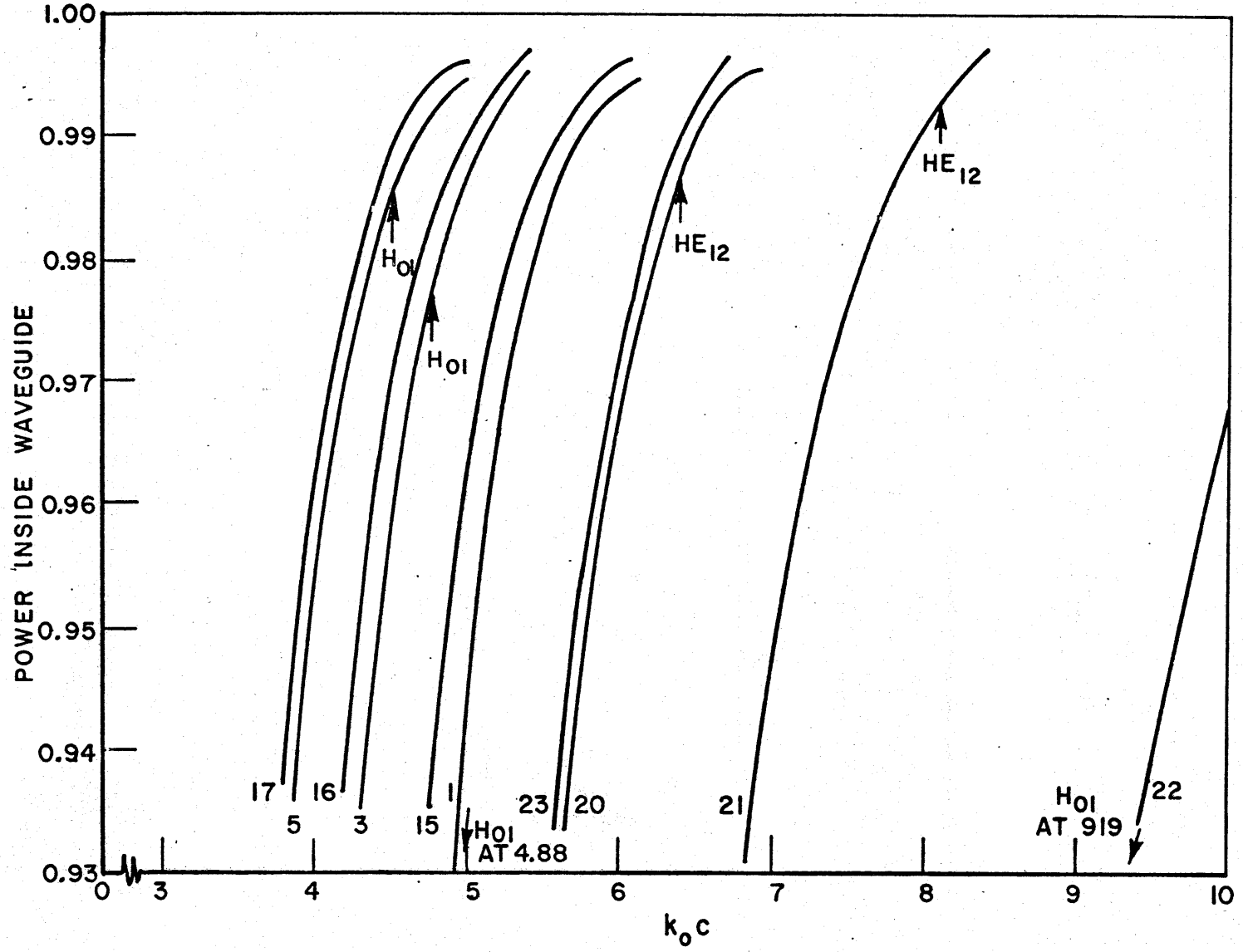

Fig. 22. Ratio of axial power transported within coaxial dielectric waveguide to total power transported. Identifying numbers refer to the geometric configurations specified in Table I. ε_1=2.55, ε_2=1.03, ε_3=2.55, $\tan\delta_3$=.0002.

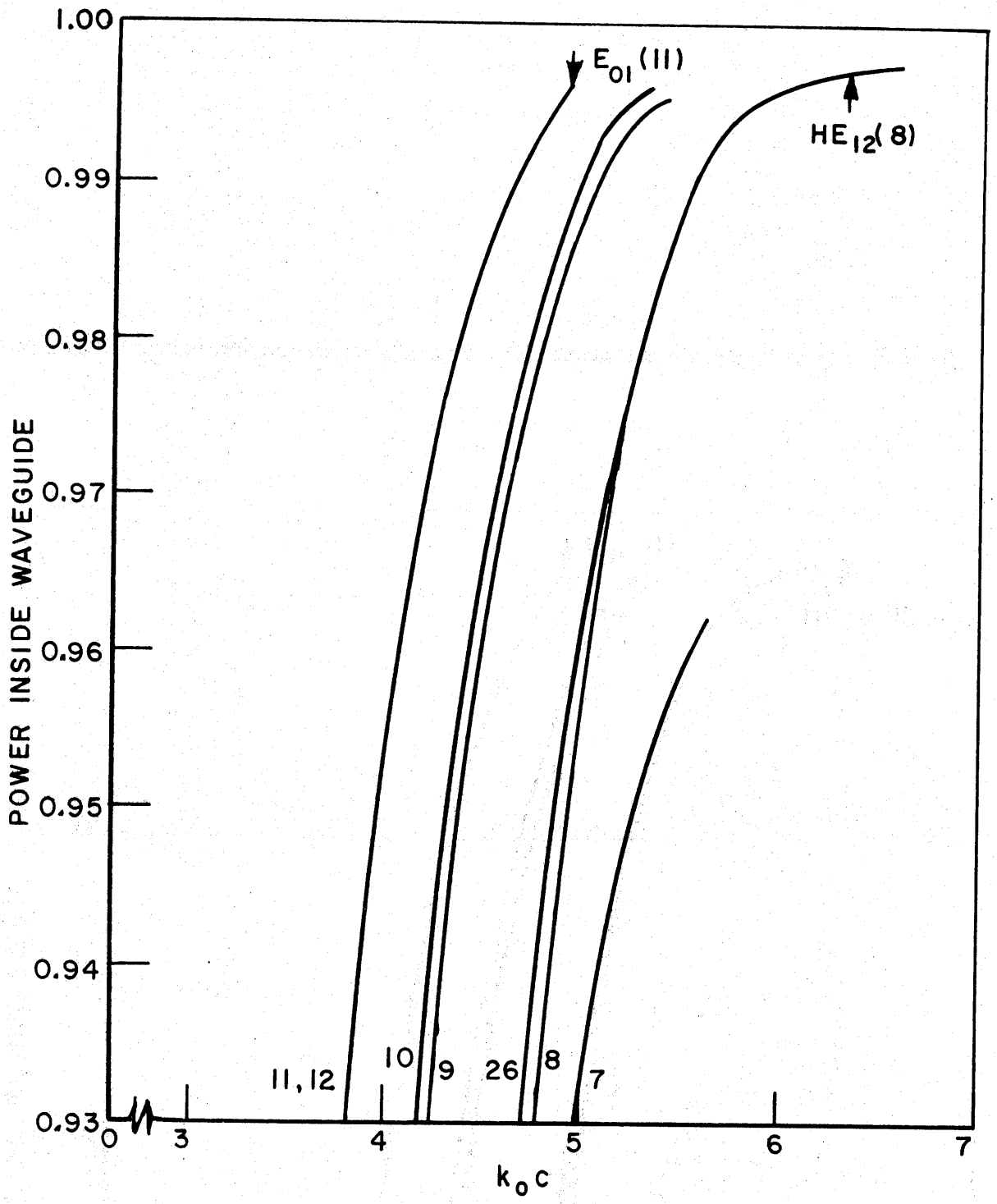

Fig. 23. Ratio of axial power transported within coaxial dielectric waveguide to total power transported. Identifying numbers refer to the geometric configurations specified in Table I. ε_1=2.55, ε_2=1.03, ε_3=2.00, $\tan\delta_3$=.0002.

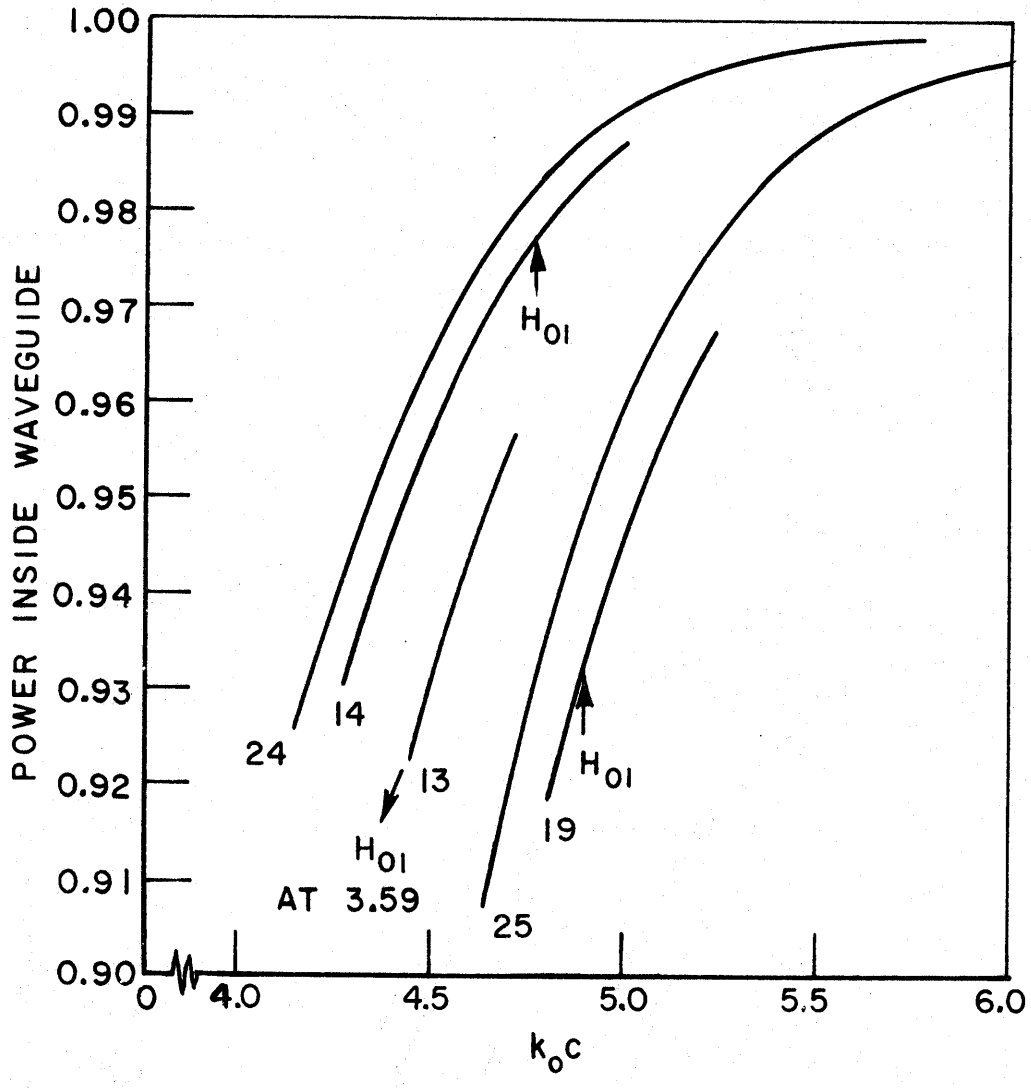

Fig. 24. Ratio of axial power transported within coaxial dielectric waveguide to total power transported. Identifying numbers refer to the geometric configurations specified in Table I. ε_1=2.55, ε_2=1.03, ε_3=4.00, $\tan\delta_3$=.04.

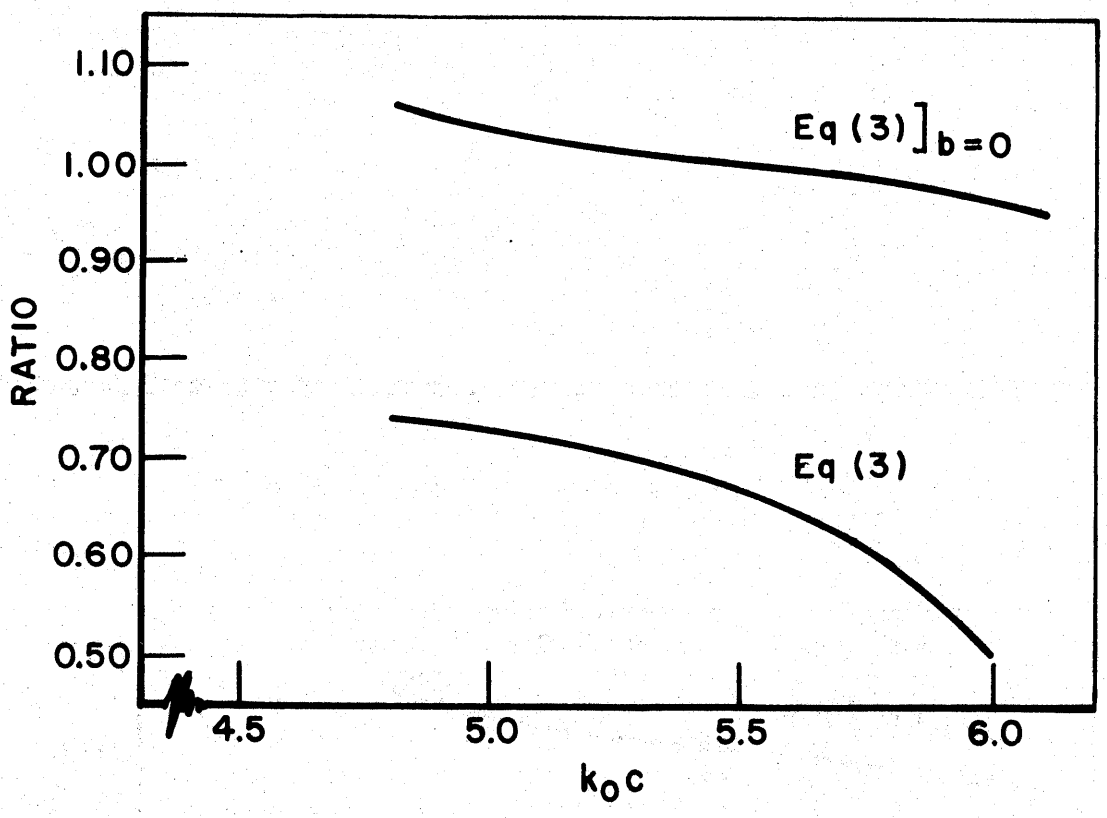

Fig. 25. Evaluation of Eq. (3) for configuration 15 of Table I.

2. A center rod radii ratio (a/c) somewhere in the range 0.15 - 0.25 may be close to optimum for the dielectric configurations considered.

3. A lossy outer layer ($\varepsilon_3 = 4.00$, $\tan \delta_3 = .04$) has prohibitively high loss.

4. In the operating band, the coaxial dielectric guide phase characteristic is much more linear than for a similar rectangular metallic guide.

5. As previously indicated, loss is a monotone increasing function with frequency.

A comparison of attenuation characteristics with those of rectangular waveguides was made. Configurations 15 and 21 were chosen, from the standpoint of bandwidth and loss respectively. For configuration 15, $k_o\ c = 5.5$ was placed at 10 GHz. This gives an outer radius $c = 1.03$ inches, where $a/c = 0.25$ and $b/c = 0.99$. For configuration 21, $k_o\ c = 7.3$ was placed at 10 GHz and 35 GHz. This gives outer radii of 1.37 and 0.39 inches for the two frequencies; also, $a/c = 0.15$ and $b/c = 0.99$. The results are shown in Fig. 21. It appears that if low dielectric loss materials are used ($\tan \delta \approx .0002$) then coaxial dielectric guides can be designed with loss characteristics similar to those of metallic rectangular guides over a somewhat narrower operating band.

We should make two comments concerning the loss tangents. The comparison in Fig. 21 was made with an assumed $\tan \delta = .0002$. The attenuation in db per foot scales linearly with loss tangent; i.e., if $\tan \delta = .0004$, then the loss per unit length would be doubled. Secondly, it is probable that the loss tangent for Styron C-176 exceeds .0002 at 35 GHz.

TABLE II
WAVEGUIDE BANDWIDTHS FOR RADII RATIO b/c = 0.99

Config. No.	a/c	$k_o\ c$ range	Band
(2.55 - 1.03 - 2.55)			
17	0.35	3.7 - 5.1	1.38:1
16	0.30	4.2 - 5.9	1.40:1
15	0.25	4.7 - 6.7	1.42:1
23	0.20	5.5 - 7.2	1.31:1
21	0.15	6.8 - 8.0	1.18:1
(2.55 - 1.03 - 2.00)			
26	0.25	4.7 - 7.0	1.49:1
(2.55 - 1.03 - 4.00)			
25	0.25	4.7 - 6.1	1.30:1

REFERENCES

1. American Institute of Physics Handbook, 3rd Ed., (1972) pp. 5-131,132.